J|A|C|S
ARTICLES

Published on Web 05/07/2008

Sodium Alanate Nanoparticles − Linking Size to Hydrogen Storage Properties

Cornelis P. Baldé, Bart P.C. Hereijgers, Johannes H. Bitter,* and Krijn P. de Jong*

Inorganic Chemistry and Catalysis, Department of Chemistry, Utrecht University, 3584 CA Utrecht, The Netherlands

Received November 28, 2007; E-mail: k.p.dejong@uu.nl; j.h.bitter@uu.nl

Abstract: Important limitations in the application of light metal hydrides for hydrogen storage are slow kinetics and poor reversibility. To alleviate these problems doping and ball-milling are commonly applied, for $NaAlH_4$ leading to particle sizes down to 150 nm. By wet-chemical synthesis we have prepared carbon nanofiber-supported $NaAlH_4$ with discrete particle size ranges of 1−10 μm, 19−30 nm, and 2−10 nm. The hydrogen desorption temperatures and activation energies decreased from 186 °C and 116 kJ·mol^{-1} for the largest particles to 70 °C and 58 kJ·mol^{-1} for the smallest particles. In addition, decreasing particle sizes lowered the pressures needed for reloading. This reported size-performance correlation for $NaAlH_4$ may guide hydrogen storage research for a wide range of nanostructured light (metal) hydrides.

1. Introduction

Hydrogen storage materials need to fulfill strict requirements with respect to safety, capacity, and kinetics for on-board application.[1] Lightweight metal hydrides are considered as storage media, but kinetic constraints limit their application. A promising approach to address this issue is to reduce the particle size of the metal hydride to the nanometer range, resulting in enhanced kinetics without the need of a catalyst.[2,3] Nanoparticles often display modified behavior compared to bulk particles and are applied for instance in catalysis,[4,5] chemical sensors,[6] or optics.[7,8] Here, we focus on size effects of sodium alanate ($NaAlH_4$) particles. The structure and hydrogen storage properties of $NaAlH_4$ have been studied extensively over the past 10 years as can be concluded from several reviews.[9−12] This complex hydride can, therefore, be considered as a model system to arrive at more generally applicable conclusions on size effects for hydrogen storage materials.

Particle sizes of metal hydrides are usually decreased by ball milling, for $NaAlH_4$ preferably in the presence of a Ti-based catalyst.[13−15] However, with that method the particle size is difficult to control, the size distribution is broad, and the smallest particle size achievable is typically 150 to 200 nm for $NaAlH_4$.[15] Therefore another preparation method is needed to study particles smaller than 150 nm. Nanoparticles are regularly synthesized by deposition of a metal precursor onto a support material in heterogeneous catalysis.[16,17] In the field of hydrogen storage, this approach has been demonstrated to facilitate H_2 desorption rates for $NaAlH_4$,[2] nanoscaffolded NH_3BH_3,[3,18] and $LiBH_4$.[19,20] However, the particle size of the hydrides used in those studies was not reported. Here, we present an extensive study using alternative preparation routes, characterization of the $NaAlH_4$ particle size, and the effect of particle size on hydrogen storage properties. The $NaAlH_4$ particles were supported on Carbon Nanofibers (CNF). Particle sizes were determined using Scanning Electron Microscopy (SEM), Transmission Electron Microscopy (TEM), and quantitative X-ray Photoelectron Spectroscopy (XPS). The hydrogen desorption properties of the samples were linked to the particle sizes, and H_2 absorption characteristics were compared to those of ball milled $TiCl_3$−$NaAlH_4$.

(1) Schlapbach, L.; Züttel, A. *Nature* **2001**, *414*, 353–358.
(2) Baldé, C. P.; Hereijgers, B. P. C.; Bitter, J. H.; de Jong, K. P. *Angew. Chem., Int. Ed.* **2006**, *45*, 3501–3503.
(3) Gutowska, A.; Li, L.; Shin, Y.; Wang, C. M.; Li, X. S.; Linehan, J. C.; Smith, R. S.; Kay, B. D.; Schmid, B.; Shaw, W.; Gutowski, M.; Autrey, T. *Angew. Chem., Int. Ed.* **2005**, *44*, 3578–3582.
(4) Bezemer, G. L.; Bitter, J. H.; Kuipers, H. P. C. E.; Oosterbeek, H.; Holewijn, J. E.; Xu, X.; Kapteijn, F.; van Dillen, A. J.; de Jong, K. P. *J. Am. Chem. Soc.* **2006**, *128*, 3956–3964.
(5) Bell, A. T. *Science* **2003**, *299*, 1688–1691.
(6) Kong, J.; Franklin, N. R.; Zhou, C.; Chapline, M. G.; Peng, S.; Cho, K.; Dai, H. *Science* **2000**, *287*, 622–625.
(7) Xi, J.-Q.; Kim, J. K.; Schubert, E. F. *Nano Lett.* **2005**, *5* (7), 1385–1387.
(8) Tong, L.; Lou, J.; Gattass, R.; He, S.; Chen, X.; Liu, L.; Mazur, E. *Nano Lett.* **2005**, *5* (2), 259–262.
(9) Schüth, F.; Bogdanovic, B.; Felderhof, M. *Chem. Commun.* **2004**, *37*, 2249–2258.
(10) Grochala, W.; Edwards, P. P. *Chem. Rev.* **2004**, *104* (3), 1283–1315.
(11) Orimo, S.; Nakamori, Y.; Eliseo, J. R.; Züttel, A.; Jensen, C. M. *Chem. Rev.* **2007**, *107* (10), 4111–4132.
(12) Bogdanovic, B.; Eberle, U.; Felderhoff, M.; Schüth, F. *Scr. Mater.* **2007**, *56*, 813–816.
(13) Bogdanovic, B.; Felderhoff, M.; Pommerin, A.; Schüth, F.; Spielkamp, N. *Adv. Mater.* **2006**, *18*, 1198–1201.
(14) Fichtner, M.; Fuhr, O.; Kircher, O.; Rothe, J. *Nanotechnology* **2003**, *14* (7), 778–785.
(15) Brinks, H. W.; Hauback, B. C.; Srinivasan, S. S.; Jensen, C. M. *J. Phys. Chem. B* **2005**, *109*, 15780–15785.
(16) Pan, X.; Fan, Z.; Chen, W.; Ding, Y.; Luo, H.; Bao, X. *Nat. Mater.* **2007**, *6*, 507–511.
(17) Sietsma, J. R. A.; Meeldijk, J. D.; den Breejen, J. P.; Versluijs-Helder, M.; van Dillen, A. J.; de Jongh, P. E.; de Jong, K. P. *Angew. Chem., Int. Ed.* **2007**, *46*, 4547–4549.
(18) Feaver, A.; Sepehri, S.; Shamberger, P.; Stowe, A.; Autrey, T.; Cao, G. *J. Phys. Chem. B* **2007**, *111* (26), 7469–7472.
(19) Züttel, A.; Wenger, P.; Rentsch, S.; Sudan, P.; Mauron, P.; Emmenegger, C. *J. Power Sources* **2003**, *118*, 1–7.
(20) Vajo, J. J.; Olson, G. L. *Scr. Mater.* **2007**, *56* (10), 829–834.

2. Experimental Section

Fishbone CNF of 20−30 nm in diameter were grown from 5 wt % Ni/SiO_2 (425−850μm SiO_2 particles) using H_2/CO as described by Van der Lee et al.[21] After CNF synthesis, SiO_2 was removed by refluxing the product in 1 M KOH. Subsequently, Ni was removed by refluxing the product in fresh concentrated HCl. After each refluxing step, the CNF were thoroughly washed with demineralized water. Finally, the CNF were dried in an inert atmosphere at 500 °C and stored in a glovebox for further use. The CNF prepared in this way contained a low concentration (<0.02 $mmol \cdot g^{-1}$) of oxygen-containing groups on the surface and had a specific surface area of 130 $m^2 \cdot g^{-1}$.[22]

All further sample handling was conducted under a dry and inert atmosphere using either Schlenk equipment or an N_2 filled glovebox with a circulation purifier. $NaAlH_4$ (90% Sigma Aldrich) was purified by dissolving it in dried THF followed by filtration to remove insoluble contaminants. The pure Alanate was obtained as a white powder after evaporation of the THF under reduced pressure. It was stored in a glovebox and used within 1 day.

$NaAlH_4$ was deposited on CNF by pore volume (1 $mL \cdot g^{-1}$) impregnation using dried THF as a solvent. Samples with $NaAlH_4$ loadings of 2 and 8 wt % were prepared by adapting the concentration of $NaAlH_4$ in the impregnation solution. Both samples were dried at reduced pressure (6 mbar) while heating from −40 to −15 °C over a period of 3 h; this is denoted as low temperature drying. In addition, a sample was prepared with a loading of 9 wt % which was dried at room temperature for 5 min at 6 mbar (denoted as room-temperature drying).

Temperature Programmed Desorption (TPD) of H_2 was performed using a Micromeritics AutoChem II 2920. A 200 to 400 mg amount of sample was loaded in the reactor and heated, in a 25 mL/min Ar flow while heating from −20 to 300 °C. Reloading of the samples was performed in a high pressure magnetic suspension balance from Rubotherm.[23,24] For "19−30 nm $NaAlH_4$", 250 mg sample were loaded in the balance. For ball milled $TiCl_3-NaAlH_4$ (prepared via procedure described by Haiduc et al.,[25] Ti/Al = 0.05 at/at) 4 mg were loaded. Prior to the uptake measurement, the sample was desorbed at 0.1 bar H_2 pressure (99.999 % purity) at 250 °C. Next, the temperature was lowered to the absorption temperature (115 °C) and equilibrated for 1 h. H_2 uptake was monitored by the weight increase of the sample during the subsequent pressure increase (1.38 $bar \cdot min^{-1}$) to 100 bar H_2 pressure. Hydrogen uptake and desorption were determined after subtracting the weight changes of an empty sample holder and applying a buoyancy correction due to the volume of the sample.

For SEM studies, samples were crushed by mortar and pestle in a glovebox. SEM studies were performed using an FEI XL30 FEG electron microscope equipped with an EDX detector. The crushed sample was fixed to a double-sided carbon tape and transported in an N_2 atmosphere to the microscope. Mounting the sample into the microscope involved brief (less than 1 min) exposure to air. In SEM studies we have limited beam damage of the sodium alanate particles by beam focusing on a certain part of the specimen followed by moving to a fresh part of the sample that was directly imaged. HR-TEM and STEM images were obtained using a Tecnai 20 (200 kV) equipped with an EDX and an HAADF detector. All samples for TEM were desorbed at 300 °C prior to analysis after which they were passivated in air and mounted to the sample holder. The rationale for sample desorption and passivation relates to inevitable beam damage (particle instability and Na-evaporation) to sodium alanate in TEM.[26–28] Desorption and passivation appeared to maintain particle size (see section 3.1) although particle morphology may have changed.

X-ray Photoelectron Spectroscopy (XPS) spectra were acquired from a Perkin-Elmer (PHI) model 5580 spectrometer using Al Kα radiation. Samples were desorbed at 300 °C, passivated in ambient air, crushed, and pressed on double-sided carbon tape. Using the Al/C atomic ratio it was found that the details of passivation (duration, oxygen concentration) had little effect if any (<10% relative) on the ratios obtained. Shirley backgrounds were subtracted from the raw data to obtain the areas of the C_{1s}, Al_{2p}, and Na_{1s} signals. The inelastic mean free path of photoelectrons generated in $NaAlH_4$ is very small, i.e., 3.1 nm for C_{1s}, 2.6 nm for Al_{2p}, and 1.1 nm for Na_{1s}. Thus, the intensity ratios Al_{2p}/C_{1s} and Na_{1s}/C_{1s} together with the loading and CNF specific surface area were used to calculate the dispersion of Na and Al on the CNF based on the model by Kuipers et al.[29,30] Particle sizes obtained earlier for Co on CNF[4] with this model were in good agreement with TEM, EXAFS, and H_2 chemisorption results.

In situ powder X-ray diffraction data were recorded on a Bruker-AXS D-8 diffractometer using $Co_{K\alpha 1,2}$ radiation. The sample was crushed, loaded in an Anton-Paar reaction chamber in the glovebox, closed, and transported to the diffractometer. The reaction chamber was connected to a gas system, and measurements were carried out in flowing N_2 with a ramp of 2 $°C \cdot min^{-1}$ to 250 °C.

3. Results and Discussion

3.1. Preparation and Structure of Nano-$NaAlH_4$. The CNF support material used in this study consisted of entangled fibers with diameters between 20 and 30 nm resulting in a porous skein. Figure 1A displays a typical SEM micrograph of a CNF skein to illustrate its morphology. The CNF skeins were impregnated with a solution of $NaAlH_4$ in THF until the pore volume was completely filled. $NaAlH_4$ was deposited on the CNF by subsequent drying. The drying conditions (temperature) and $NaAlH_4$ loading determined the size of $NaAlH_4$ particles on the CNF. Since the samples used in SEM have been exposed to air, particle morphology may have been affected. The size of the particles, however, was qualitatively confirmed by XRD patterns (data not shown) that displayed sharp lines and thus particles > 100 nm. As shown below for much smaller particles, the sizes obtained from SEM/TEM were quantitatively supported by XRD and XPS. Drying at room temperature under reduced pressure of 9 wt % $NaAlH_4$ on CNF resulted in particles varying from 1 μm (Figure 1B) to 10 μm (Figure 1C) at the outer surface of the CNF skeins. This sample will be referred to as "1−10 μm $NaAlH_4$".

A second sample with a comparable loading of 8 wt % $NaAlH_4$ was dried at low temperature (−40 °C to −15 °C). In that sample, SEM did not reveal the presence of large $NaAlH_4$ particles (Figure 1D). However, the fibers, shown in Figure 1D for a relatively porous part of the sample, had been thickened

(21) van der Lee, M. K.; van Dillen, A. J.; Bitter, J. H.; de Jong, K. P. *J. Am. Chem. Soc.* **2005**, *127* (39), 13573–13582.
(22) Toebes, M. L.; van Heeswijk, E. M. P.; Bitter, J. H.; van Dillen, A. J.; de Jong, K. P. *Carbon* **2004**, *42* (2), 307–315.
(23) Dreisbach, F.; Seif, R.; Lösch, H. W. *J. Therm. Anal. Calorim.* **2003**, *71*, 73–82.
(24) Lösch, H. W.; Kleinrahm, R.; Wagner, W. *Neue Magnetschwebewaagen für gravimertrische Messungen in der Verfahrentechnik;* VDI-Verslag: Düsseldorf, 1994.
(25) Haiduc, A. G.; Stil, H. A.; Schwarz, M. A.; Paulus, P.; Geerlings, J. J. C. *J. Alloys Compd.* **2005**, *393* (1−2), 252–263.
(26) Graham, D. D.; Culnane, L. F.; Sulic, M.; Robertson, C. M. J. I. M. *J. Alloys Compd.* **2007**, *446−447*, 255–259.
(27) Andrei, C. M.; Walmsley, J. C.; Brinks, H. W.; Holmestad, R.; Srinivasan, S. S.; Jensen, C. M.; Haubac, B. C. *Appl. Phys. A* **2005**, *80*, 709–715.
(28) Felderhoff, M.; Klementiev, K.; Grunert, W.; Spliethoff, B.; Tesche, B.; Colbe, J. M. B. V.; Bogdanovic, B.; Hartel, M.; Pommerin, A.; Schüth, F.; Weidenthaler, C. *Phys. Chem. Chem. Phys.* **2004**, *6*, 4369–4374.
(29) Kuipers, H. P. C. E. *Solid State Ion.* **1985**, *16*, 15–21.
(30) Kuipers, H. P. C. E.; Leuven, H. C. E. V.; Visser, W. M. *Surf. Interface Anal.* **1986**, *8* (6), 235–242.

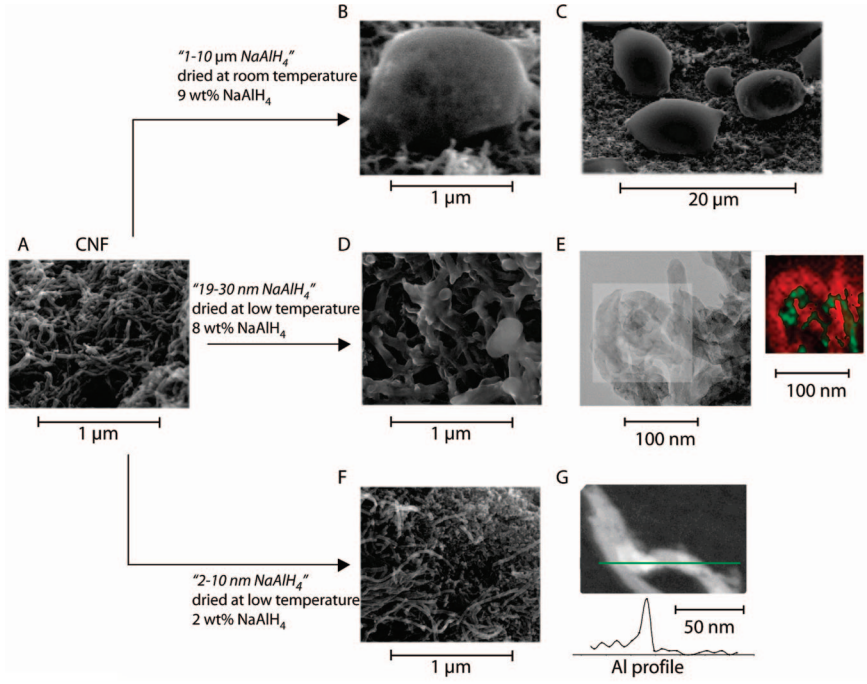

Figure 1. Overview of $NaAlH_4$/CNF samples. (A) CNF skein prior to impregnation; (B and C) SEM micrographs of "1−10 μm $NaAlH_4$"; (D) SEM micrograph of "19−30 nm $NaAlH_4$"; (E) TEM and an EDX elemental map of highlighted region (C in red and Al in green) for "19−30 nm $NaAlH_4$" after desorption; (F) SEM micrograph of "2−10 nm $NaAlH_4$"; (G) TEM micrographs with Al profile of "2−10 nm $NaAlH_4$" after desorption.

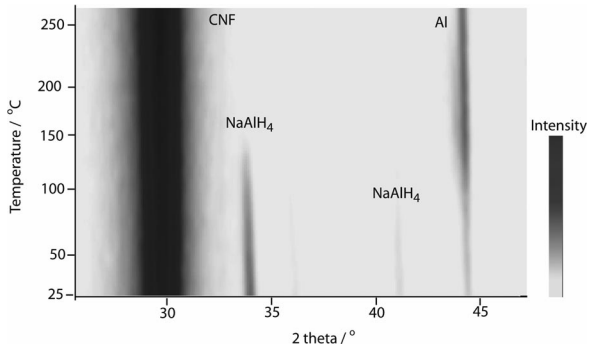

Figure 2. In situ X-ray diffraction of "19−30 nm $NaAlH_4$" with heating ramp of 2 °C·min^{-1}.

by $NaAlH_4$ deposition suggesting $NaAlH_4$ present on the individual fibers. A particle size could not be derived from SEM but required XRD, TEM, and XPS of the sample after hydrogen desorption; i.e., $NaAlH_4$ decomposed to Al and NaH.[31] Whether the particle size of the material after desorption represented the original particle size has been verified with XRD.

Figure 2 shows a two-dimensional plot of the XRD patterns of the 8 wt% $NaAlH_4$ as a function of the desorption temperature. In the fresh material the diffractions of CNF, $NaAlH_4$, and Al were detected. During heating the intensity of the $NaAlH_4$ diffractions decreased and became zero above 150 °C. The disappearance of the $NaAlH_4$ diffractions was paralleled by an increase in the Al diffraction line. From the width of the $NaAlH_4$ and Al diffraction lines it was established that both the $NaAlH_4$ and Al particles were on average 22 nm. Therefore, the Al particle size obtained after decomposition by all techniques coincided with the original $NaAlH_4$ particle size.

Figure 1E shows a TEM micrograph of this sample after desorption together with the Al and C elemental maps of the highlighted region. The carbon map followed the structure of the fibers as expected. Al domains were detected on the fibers

Table 1. Atomic ratios and particle size obtained by XPS

$NaAlH_4$ loading (wt %)	Al/C (at/at)	Na/C (at/at)	Al (*d*/nm)
2	0.0055	0.032	2
8	0.0071	0.059	19

with sizes between 20 and 30 nm. The particle size of Al was additionally determined using quantitative XPS, which was based on the Al/C ratio of desorbed $NaAlH_4$ samples, specific surface area of the CNF and $NaAlH_4$ loading.[29,30] The atomic Al/C and Na/C ratios are listed in Table 1. When the model was used assuming hemispherical particles, the Al particles size was calculated to be 19 nm (Table 1). The high atomic Na/C suggested that NaH was highly, possibly atomically, dispersed. The Al particle size is in agreement with the 20−30 nm particle size range obtained from TEM (Figure 1E), illustrating the suitability of the XPS model. The sample will be referred to as "19−30 nm $NaAlH_4$".

The higher dispersion of NaH than that of Al, as inferred from XPS, is in agreement with the in situ diffraction experiment shown in Figure 2. It was observed that NaH was XRD amorphous, whereas Al showed diffraction lines. A possible cause for the higher dispersion is that the interaction of NaH with the CNF support is considerable larger than the interaction of Al with the CNF. If a carbon support is absent, NaH and Al will not be highly dispersed. Consequently, unsupported $NaAlH_4$ upon desorption will form large NaH and Al particles, as was found in other studies for bulk samples with TEM,[28] SEM,[32] and XRD.[33]

In the third sample, the fibers were impregnated with a lower concentration of $NaAlH_4$ in solution. The impregnated material

(31) When $NaAlH_4$ is heated it decomposes via the following reactions: $NaAlH_4 \leftrightarrow {}^1/_3Na_3AlH_6 + {}^2/_3Al + H_2 \leftrightarrow NaH + Al + {}^3/_2H_2$. The material after desorption was used for XPS and TEM studies since $NaAlH_4$ is not stable under the conditions which TEM and XPS measurements are performed (low pressure and ionizing radiation).

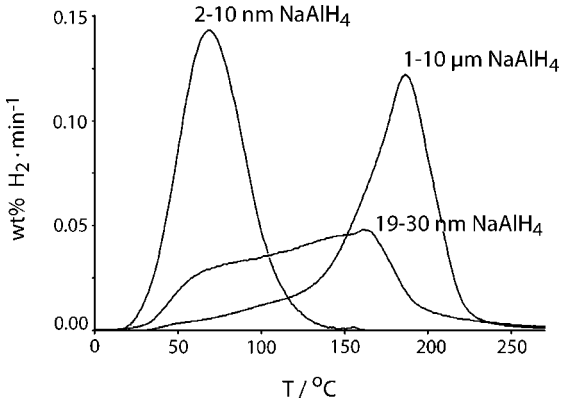

Figure 3. Temperature programmed desorption profiles of H_2 for $NaAlH_4$/CNF samples under Ar atmosphere. Heating ramp 5 °C/min.

was dried at low temperature, and the loading was 2 wt % $NaAlH_4$. SEM only detected the individual CNF fibers in this sample (Figure 1F), indicating that the $NaAlH_4$ particles were small. From STEM-EDX line scans over several single Al particles (one line scan is shown in Figure 1G) it was concluded that the upper limit of particle size was 10 nm. XPS shows that the atomic Al/C and Na/C ratios were significantly larger after normalization to the alanate loading for the 2 wt % loaded sample than those for the 8 wt% loaded sample (Table 1). This indicates that the dispersion of Al and NaH was higher in the 2 wt % loaded sample than that for the 8 wt % sample. When the same quantitative XPS model was applied, it was calculated that the 2 wt % loaded sample consisted of 2 nm Al particles. Such small Al particles could not be inferred from the EDX line scan shown in Figure 1G, as the spatial resolution was insufficient. Therefore, the combination of TEM and XPS provided a 2−10 nm particle size range, and the sample will be referred to as "2−10 nm $NaAlH_4$".

Thus, we have tuned the $NaAlH_4$ particle sizes in discrete ranges of 2−10 nm, 19−30 nm, and 1−10 μm. A detailed discussion about the influence of the preparation parameters on the particle size can be found in the Supporting Information. The effects of the particle size on H_2 desorption and absorption properties are discussed in the next section.

3.2. Size−Performance Relationship. Figure 3 shows the H_2 desorption profiles for the three CNF-supported $NaAlH_4$ samples. The temperature at the maximum desorption rate (T_{max}) was highest for "1−10 μm $NaAlH_4$" (186 °C) followed by "19−30 nm $NaAlH_4$" (164 °C) and lowest for "2−10 nm $NaAlH_4$" (70 °C). Thus, the smaller the particles, the lower the H_2 desorption temperature. The activation energy for H_2 desorption was calculated using a Kissinger analysis that is based on the shifts in T_{max} with heating rates (β) of 0.5, 1, 2, and 5 °C·min^{-1}.[34] For that, $\ln(\beta/T_{max}^2)$ was plotted versus $1/T_{max}$ (see Figure 4). The slope of the curve represents $-E_a/R$ in which R is the gas constant. From the slope in Figure 4 it was established that the E_a for H_2 desorption was 116 kJ·mol^{-1} for "1−10 μm $NaAlH_4$", which is in good agreement with reported values for uncatalyzed bulk $NaAlH_4$ (120 kJ·mol^{-1}).[35,36] Thus, the 1−10 μm $NaAlH_4$ particles showed bulk-like H_2 desorption behavior. However, the sample desorbed a small amount of H_2 below 140 °C (Figure 3). This was probably H_2 desorption from a small fraction of the $NaAlH_4$ that was smaller in size (*vide infra*).

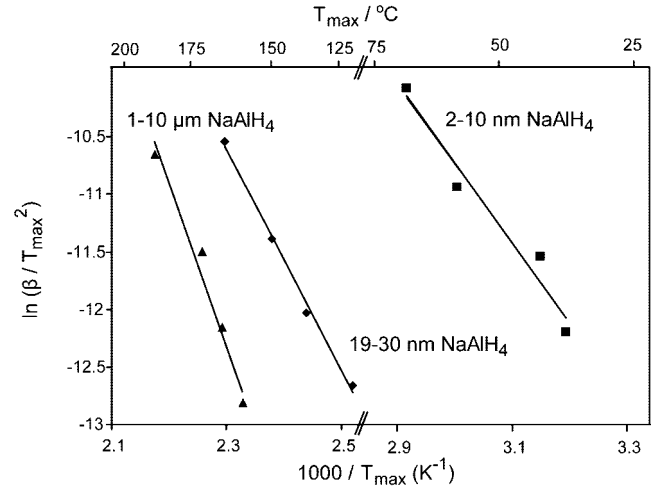

Figure 4. Kissinger plots and temperature at maximum desorption rate (T_{max}) for $NaAlH_4$ samples.

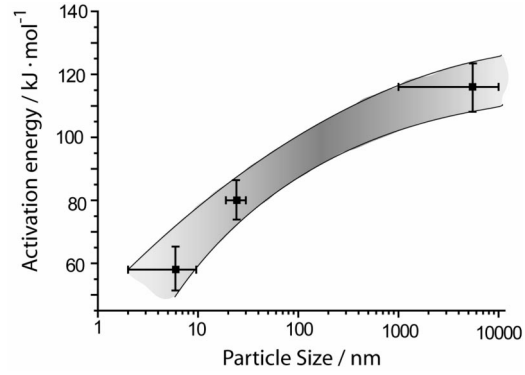

Figure 5. Relation between particle size and activation energy for hydrogen desorption from $NaAlH_4$/CNF. The spread in the particle size reflects the results from different characterization techniques, and the error bars in activation energies were obtained from linear regression analysis.

The H_2 desorption from "19−30 nm $NaAlH_4$" proceeded from 25 to 250 °C. This indicates that a broad particle size distribution was present. Most likely, H_2 evolution from 25 to 100 °C came from a fraction of particles that had a similar size as that for "2−10 nm $NaAlH_4$", since the desorption temperature coincided with that of "2−10 nm $NaAlH_4$" (Figure 3). The peak with the T_{max} at 164 °C then reflects desorption from the larger (19−30 nm) $NaAlH_4$ particles. The activation energy for H_2 desorption from these particles was 80 kJ·mol^{-1} (Figure 4) a value comparable to that of Ti-catalyzed $NaAlH_4$.[35,36] However in "19−30 nm $NaAlH_4$", no Ti was present as a catalyst. Thus, solely by reducing the particle size to the nanometer range, the activation energy decreased to the same value as ball milled $TiCl_3$−$NaAlH_4$.

The activation energy lowered to an unprecedented value of 58 kJ·mol^{-1} when the $NaAlH_4$ particle size was decreased to 2−10 nm. The relation between activation energies and particle size, i.e., a size−performance relationship, is shown in Figure 5. This correlation opens the possibility to link experiment with theoretical calculations on metal hydride nanoclusters, since now the experimental available cluster size is in the same size range

(32) Bogdanovic, B.; Brand, R. A.; Marjanovic, A.; Schwickardi, M.; Tolle, J. *J. Alloys Compd.* **2000**, *302*, 36–58.
(33) Gross, K. J.; Guthrie, S.; Takara, S.; Thomas, G. *J. Alloys Compd.* **2000**, *297*, 270–281.
(34) Kissinger, H. E. *Anal. Chem.* **1957**, *29*, 1702.
(35) Luo, W.; Gross, K. J. *J. Alloys Compd.* **2004**, *385*, 224–231.
(36) Sandrock, G.; Gross, K.; Thomas, G. *J. Alloys Compd.* **2002**, *339*, 299–308.

as those used in the theoretical studies.[37–40] But most importantly, the correlation is an advance that is applicable to other hydrogen storage materials as well.

An explanation for the reported particle size dependence for H_2 desorption can be deduced from the calculations that have been performed by Vegge on the stability of the $NaAlH_4$ surfaces.[40] It appears that open surfaces desorb hydrogen with a lower activation energy than the most densely packed (001) surface. Thus, a possible rationale for our reported particle-size dependence of the activation energy resides with a change of the structure of the $NaAlH_4$ surface with particle size. Smaller particles are expected to expose a lower fraction of (001) planes and a higher fraction of more open planes as well as corners and edges, which all lead to a lower activation energy for hydrogen desorption. Additionally, the reduction of the particle size leads to an increase in the external surface area of the alanate, which increases the number of sites where the hydrogen can desorb from. The larger number of (idententical) desorption sites is expected to enhance the rate of desorption but not to lower the activation energy.

For hydrogen desorption in (Ti-catalyzed) bulk alanate particles, the rate determining step has been established to be the mass transfer in the solid state.[41] Various studies propose different rate determining steps, such as nucleation and growth,[42] creation of vacancies,[43] or diffusion of hydrogen containing species.[44] In contrast to bulk $NaAlH_4$, hydrogen desorption from nano-$NaAlH_4$ involves a significantly shortened mass transfer length in the solid state. This might lead to a shift in the rate determining step from mass transfer in the solid state for bulk samples to hydrogen desorption from the surface for the nano-$NaAlH_4$.

The generally accepted target from the Department of Energy indicates that that an ideal automotive storage tank liberates H_2 from −30 to 85 °C. The often studied Ti-catalyzed $NaAlH_4$ has not met this target in a scale-up study.[45] However for "2−10 nm $NaAlH_4$", T_{max} ranged from 40 to 70 °C (Figures 3 and 4). These are, to the best of our knowledge, the lowest reported desorption temperatures for $NaAlH_4$ and indicate that the target is now within reach and nanosized $NaAlH_4$ has potential for application. The loading of the 2−10 nm $NaAlH_4$ particles in this paper was 2 wt % on the CNF and has to be increased for automotive applications. This might be achieved by encapsulation of the $NaAlH_4$ in nanocavities rather than the here-reported deposition of $NaAlH_4$ on the convex surface of the nanofibers.

For application, reloading of the $NaAlH_4$ after H_2 extraction must be achieved at low H_2 pressure. We studied the uptake characteristic of "19−30 nm $NaAlH_4$" as a function of H_2 pressure at 115 °C (Figure 6). For reference, the pure support material (CNF) was included which did not absorb H_2 from 0.1 to 100 bar. The "19−30 nm $NaAlH_4$" started to absorb H_2 from a relatively low H_2 pressure of 20 bar. Please note that a typical catalyzed $NaAlH_4$ (ball milled $TiCl_3$−$NaAlH_4$) absorbed H_2 starting from 45 bar (Figure 6). It was also observed that the H_2 uptake from "19−30 nm $NaAlH_4$" was lower than the total hydrogen capacity (5.6 wt % H_2). A reason for the lower loading capacity might be that the sodium hydride and aluminum particles were physically separated at the CNF surface that hampered recombination of the NaH and Al to the $NaAlH_4$. The previously mentioned encapsulation, i.e., confining the $NaAlH_4$ in nanocavities, might overcome this as well.

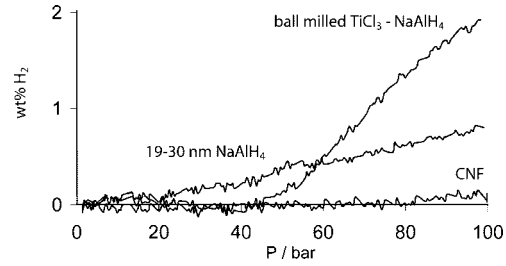

Figure 6. H_2 uptake for the first absorption step at 115 °C for 19−30 nm $NaAlH_4$ compared to the uptake from ball milled $TiCl_3$−$NaAlH_4$ and pure CNF. $\Delta P/\Delta t = 1.38$ bar·min^{-1}.

4. Conclusion

In summary, a quantitative relation is found between the activation energy for H_2 desorption and the particle size of $NaAlH_4$ varying from 116 kJ·mol^{-1} for 1−10 μm particles to 80 kJ·mol^{-1} for 19−30 nm particles, to 58 kJ·mol^{-1} for 2−10 nm particles, the latter being lower than that for Ti-catalyzed $NaAlH_4$. For the 2−10 nm particles, the H_2 desorption temperature was below 70 °C, therewith meeting the target from the Department of Energy for H_2 release. Moreover, after desorption the nano-$NaAlH_4$ showed uptake under relatively low H_2 pressures (starting at 20 bar) which can lead to the development of safer, more economical and lighter storage tanks. The nanoparticles reported in this paper were noncatalyzed, and the improvement in activation energies and absorption properties could be solely accounted by reducing the $NaAlH_4$ particle size. The size−performance relationship reported provides new avenues for other hydrides, such as other complex metal hydrides and amides, which contain a higher weight fraction of hydrogen.

Acknowledgment. The authors acknowledge Marjan Versluijs-Helder, Cor van der Spek, and Ad Mens for SEM, TEM, and XPS measurements, respectively. NWO/ACTS is acknowledged for funding (Project Number 053.61.02). Dr. Petra de Jongh and Dr. Andy Beale are thanked for their input to the manuscript. Vincent Koot and Fred Broersma are acknowledged for their assistance with TPD and Rubotherm measurements.

Supporting Information Available: Influence of $NaAlH_4$ loading and drying. This material is available free of charge via the Internet at http://pubs.acs.org.

JA710667V

(37) Marashdeh, A.; Olsen, R. A.; Løvvik, O. M.; Kroes, G. J. *Chem. Phys. Lett.* **2006**, *426*, 180–186.
(38) Marashdeh, A.; Olsen, R. A.; Løvvik, O. M.; Kroes, G. J. *J. Phys. Chem. C* **2007**, *111*, 8206–8213.
(39) Wagemans, R. W. P.; van Lenthe, J. H.; de Jongh, P. E.; van Dillen, A. J.; de Jong, K. P. *J. Am. Chem. Soc.* **2005**, *127* (47), 16675–16680.
(40) Vegge, T. *Phys. Chem. Chem. Phys.* **2006**, *8*, 4853–4861.
(41) Colbe, J. M. B. V.; Schmidt, W.; Felderhoff, M.; Bogdanovic, B.; Schüth, F. *Angew.Chem., Int. Ed.* **2006**, *45* (22), 3663–3665.
(42) Kiyobayashi, T.; Srinivasan, S. S.; Sun, D.; Jensen, C. M. *J. Phys. Chem. A* **2003**, *107*, 7671–7674.
(43) Palumbo, O.; Paolone, A.; Cantelli, R.; Jensen, C. M.; Sulic, M. *J. Phys. Chem. B* **2006**, *110*, 9105–9111.
(44) Lohstroh, W.; Fichtner, M. *Phys. Rev. B: Condens. Matter* **2007**, *75*, 184106.
(45) Jensen, J. O.; Li, Q.; He, R.; Pan, C.; Bjerrum, N. J. *J. Alloys Compd.* **2005**, *404−406*, 653–656.